Materials Science and Engineering A 528 (2011) 855–859

Contents lists available at ScienceDirect

Materials Science and Engineering A

journal homepage: www.elsevier.com/locate/msea

Boron effects on the ductility of a nano-cluster-strengthened ferritic steel

Z.W. Zhang[a,b], C.T. Liu[b,c,*], S. Guo[c], J.L. Cheng[a], G. Chen[a], Takeshi Fujita[d], M.W. Chen[d], Yip-Wah Chung[e], Semyon Vaynman[e], Morris E. Fine[e], Bryan A. Chin[b]

[a] Engineering Research Center of Materials Behavior and Design, Ministry of Education, Nanjing University of Science and Technology, Nanjing 210094, PR China
[b] Materials Research & Education Center, Auburn University, 275 Wilmore Labs, Auburn, AL 36849, USA
[c] Department of Mechanical Engineering, the Hong Kong Polytechnic University, Hung Hom, Kowloon, Hong Kong
[d] Institute for Materials Research, and World Premier International Research Center for Atoms, Molecules and Materials, Tohoku University, Sendai 980-8577, Japan
[e] Department of Materials Science and Engineering, Northwestern University, Evanston, IL 60208-3108, USA

ARTICLE INFO

Article history:
Received 2 June 2010
Received in revised form 17 August 2010
Accepted 18 October 2010

Keywords:
Nano-cluster
Ferritic steel
Boron doping
Moisture-induced embrittlement
Ductility

ABSTRACT

The mechanical properties of Cu-rich nano-cluster-strengthened ferritic steels with and without boron doping were investigated. Tensile tests at room temperature in air showed that the B-doped ferritic steel has similar yield strength but a larger elongation than that without boron doping after extended aging at 500 °C. There are three mechanisms affecting the ductility and fracture of these steels: brittle cleavage fracture, week grain boundaries, and moisture-induced hydrogen embrittlement. Our study reveals that boron strengthens the grain boundary and suppresses the intergranular fracture. Furthermore, the moisture-induced embrittlement can be alleviated by surface coating with vacuum oil.

1. Introduction

Most high-strength steels are usually martensitic. The strength of martensitic steels increases with carbon content. High carbon content, however, leads to poor ductility and weldability. This problem can be solved by using steels with low carbon content and enhancing the strength by nanoscale Cu-rich precipitates [1–5]. The precipitation of Cu-rich nanoclusters increases the strength and hardness of these alloys, accompanied by decrease in ductility and toughness [3,6]. It is well known [7] that several factors can influence the fracture mode of steels, including alloy composition, process variables, grain size, distribution and morphology of the embrittling constituent. In the case of nano-cluster strengthened ferritic steels, the relative strength of the grain boundary with respect to the matrix is expected to determine the fracture mode and hence the ductility.

Boron is known for its ability to enhance grain boundary strength and ductility of intermetallic compounds, such as Ni_3Al [8] and FeAl [9]. Boron segregation was also found to improve the low temperature ductility in bcc iron alloys and refractory metals by enhanced intergranular cohesion [10,11]. In this study, we investigated the effects of boron on the fracture mode and ductility of a Cu-rich nano-cluster strengthened ferritic steel. Moisture-induced environmental embrittlement, a potential source of embrittlement in some metals and alloys at ambient temperature, was also evaluated.

2. Experimental

Ingots were made by arc melting a mixture of 99.95% Fe, 99.8% Mn, 99.99% Ni, 99.99% Cu, 99.99% Al (wt.% purity) with and without boron doping. The concentration of boron was 0.03 wt.%. Ingots with and without B doping were remelted several times to ensure homogeneous distribution of alloying elements under a Ti-gettered Ar atmosphere. The arc-melted alloy button was then drop-cast into rods of 10 mm in diameter. The chemical composition of the as-cast steels with B doping (in wt.%) was: 0.01C; 1.42Mn; 4.14Ni; 2.49Cu; 1.00Al; 0.028B; <0.005P; 0.002S; 0.003Ni; <0.01Si; and balance Fe. The as-cast specimens were heated at 1000 °C in air for 1 h and then quenched in water. The as-quenched specimens were aged at 500 °C for 10 and 200 h, respectively. Sheet tensile samples were prepared by electro-discharge machining (EDM) and were carefully polished to remove the damaged surface layer. Tensile specimens with gage sizes of 12.5 mm × 3 mm × 0.75 mm were tested at a strain rate of 0.04 s^{-1}. Tensile tests were performed on Instron 5565 testing machine at room temperature in air. Selected

* Corresponding author at: Materials Research & Education Center, Auburn University, 275 Wilmore Labs, Auburn, AL 36849, USA. Tel.: +1 852 2766 6644; fax: +1 852 2365 4703.
E-mail address: mmct8tc@inet.polyu.edu.hk (C.T. Liu).

0921-5093/$ – see front matter © 2010 Elsevier B.V. All rights reserved.
doi:10.1016/j.msea.2010.10.058

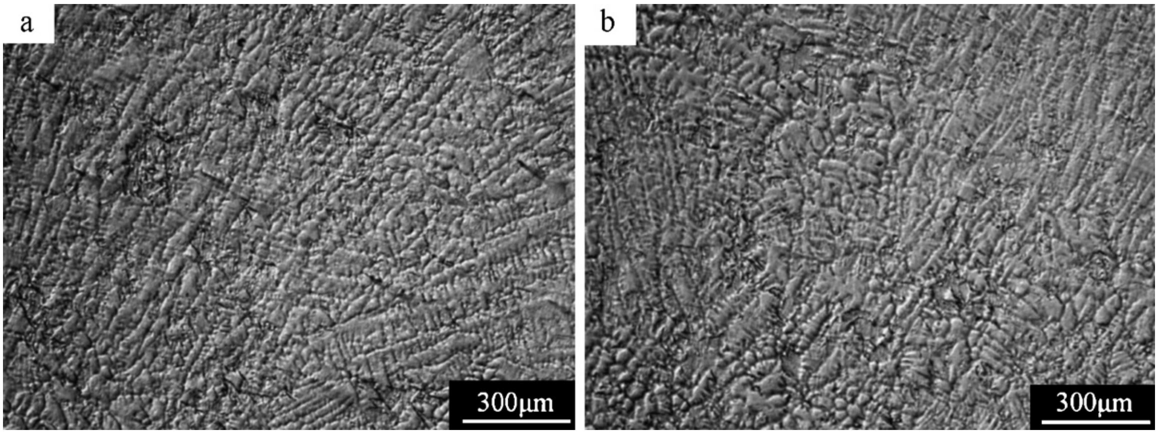

Fig. 1. Optical microstructures of the as-cast ingots after water-quenching: (a) B-doped steel and (b) B-free steel.

B-doped and B-free specimens after water-quench and aging at 500 °C for 10 h were coated with vacuum oil before tensile testing. The yield strength was determined by the 0.2% offset plastic strain method. Hardness measurements were conducted under a 500 g applied load, and the average hardness (VHN) of a particular sample was reported from measurement over ten locations. X-ray diffraction (XRD) was used to determine the phase components of the specimens. Optical microscopy (OM), scanning electron microscope (SEM) and scanning transmission electron microscopy (STEM) were used to characterize the microstructure of the specimens. The fracture surfaces were examined by SEM, and the phase compositions were determined by microprobe analysis.

3. Results

Fig. 1 shows the optical microstructures of the as-cast ingots with and without B doping after water quenching. The optical observations showed that large dendrites are clearly visible after water quenching. The prolonged aging does not change the microstructure significantly for both specimens. XRD results show that the specimen consists of single ferrite phase after heating at 1000 °C for 1 h and quenching into water. Fig. 2(a) and (b) shows the SEM backscatter electron images (BEIs) of water-quenched specimens with and without B doping, respectively. In the specimen with B doping, ~2.5 μm sized B-rich second phase particles precipitated. These particles can be found even after aging for 200 h at 500 °C. Microprobe analysis shows the composition of these particles to be $(FeAl)_2B$. Fu et al. also found that the water-quenching can induce the formation of eutectic Fe_2B along the grain boundaries in B-containing cast steels [12]. These particles were not found in specimens without B doping.

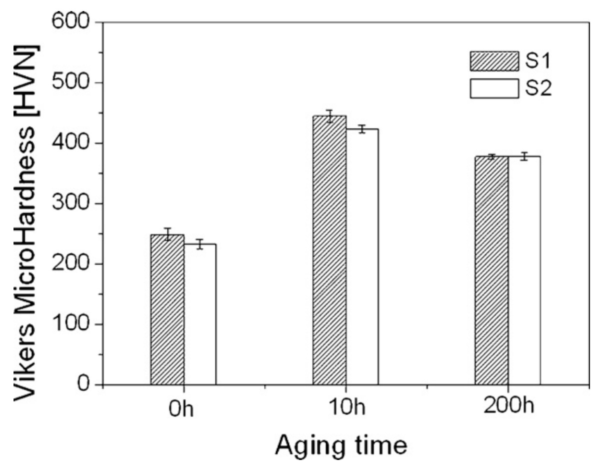

Fig. 3. Vikers microhardness (HVN) versus aging time for B-doped (S1) and B-free (S2) steels after various heat treatments.

The variation of microhardness with aging time of both B-doped and B-free steels are shown in Fig. 3. For both steels, there was a low VHN value in the as-quenched condition. The VHN was increased substantially after water-quenching and aging for 10 h. Prolonging the aging time to 200 h, the hardness decreased slightly again.

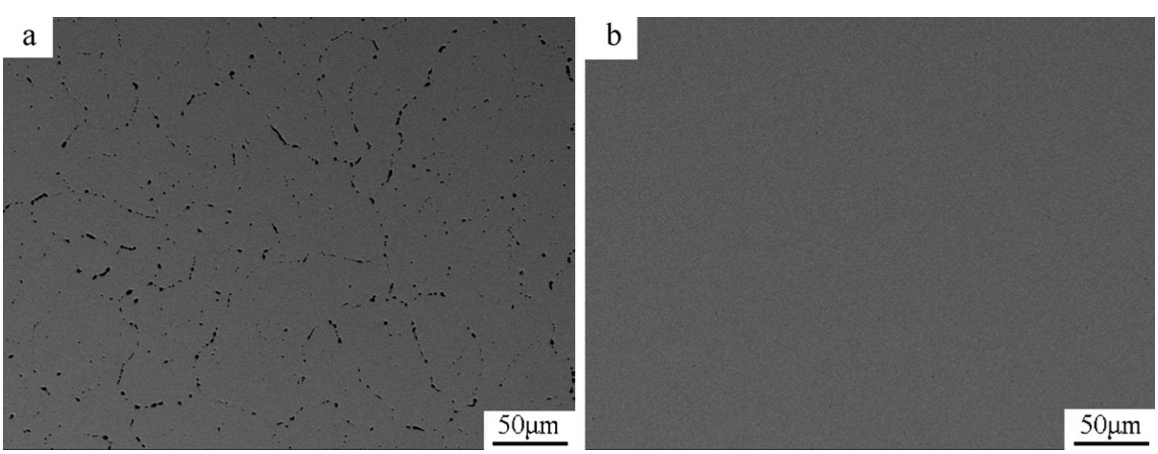

Fig. 2. Backscattered electron images showing (a) the distribution of boride particles $(FeAl)_2B$ along grain boundaries in B-doped steel and (b) the absence of boride particles in B-free steel.

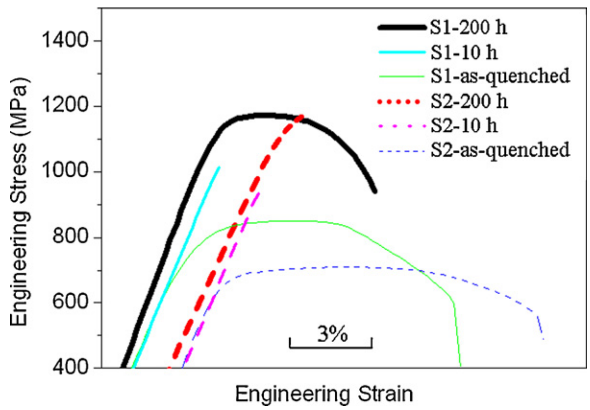

Fig. 4. Engineering stress versus engineering strain curves for B-doped (S1) and B-free (S2) steels after various heat treatments.

Results of tensile testing of specimens with and without B doping are shown in Fig. 4. In the water-quenched condition, the B-doped steel has a higher yield strength and slightly smaller elongation as compared with B-free steel. This is due to the precipitation of boride particles in the B-doped specimen. Fu et al. [12] also found that the borides distributed along the grain boundaries can enhance the hardness and strength. After water-quenching and aging for 200 h, the B-doped steel sustains a plastic strain of about 8% before failure, compared with ~1% for the B-free steel. Both steels have a similar yield strength of about 1100 MPa. This is in consistence with the microhardness results as shown in Fig. 3. However, both steels with and without B doping after water quenching and aging at 500 °C for 10 h showed a similar brittle fracture without macroscopic yielding. This is because in this aging condition, nanocluster precipitation induced the highest hardness in steels as shown in Fig. 3. The high hardness of the matrix induced by nanocluster precipitation makes the steels more sensitive to environmental embrittlement, leading to a fracture prior to macroscopic yielding.

Fig. 5 compares the tensile properties of the specimens with and without oil coating on surface. The specimens were water-quenched and then aged at 500 °C for 10 h (the most severe embrittlement condition). It is apparent that the yield strength and ductility of both B-doped and B-free steels increase significantly with oil coating before tensile testing. Both alloys without oil coating essentially fractured prior to macroscopic yielding. However, the elongation increased to ~2% and ~1% respectively for the steels with and without B doping after oil coating, respectively. This comparison demonstrates that the ductility of these steels is sensitive to oil coating, with an improved ductility after oil coating. The yield strength of oil-coated specimens reached 1218 MPa and 1163 MPa, respectively, with increased ductility while the microhardness tests showed no effect of oil coating on hardness for both B-doped and B-free steels. The inset in Fig. 5 shows a Z-contrast STEM image indicating the precipitation of Cu-rich nanoclusters in a B-doped specimen after aging at 500 °C for 10 h. These nearly spherical clusters with sizes from 2-2.5 nm are distributed uniformly in the matrix, which is the main source of strengthening in these steels.

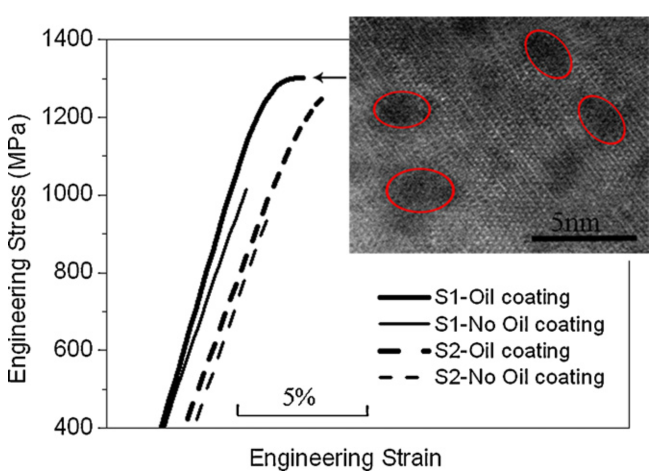

Fig. 5. Engineering stress vs engineering strain curves for B-doped (S1) and B-free (S2) steels with and without oil coating before tensile testing. All the specimens were water-quenched and then aged at 500 °C for 10 h. Z-contrast STEM (insert) showing the precipitation of nanoclusters in B-doped specimen aged at 500 °C for 10 h. The nanoclusters in Z-contrast STEM picture were circled.

To explore the effect of B doping on the fracture mode, the surfaces of the fractured samples were examined by SEM and shown in Fig. 6. As can be seen, B doping does not affect the fracture mode of the steels after water quenching. Both B-doped and B-free steels show the same micro-void coalescence fracture mode, indicating a ductile fracture. However, B doping does affect the fracture mode significantly when the specimens were water-quenched and aged at 500 °C for 10 h and 200 h. The B-doped specimen shows a micro-void coalescence fracture mode accompanied with fine network of shear dimples and secondary cracks, while fractured surface of the B-free specimen shows a combination of intergranular and cleavage facets. After aging for 10 h, the specimen with B doping fails by complete cleavage fracture while the fractured surface of the specimen without B doping is a combination of intergranular and cleavage facets, similar with that of the aged sample at 500 °C for 200 h. The oil-coating for both B-doped and B-free steels does not affect the fracture mode significantly.

4. Discussion

Based on the above results, it is clear that B doping significantly affects the mechanical behavior of the nano-cluster-strengthened ferritic steel investigated. In the water-quenched condition, there is insufficient time for the formation of a significant concentration of nanoclusters, so no appreciable strengthening is observed. In this case, the effect of boron on the grain boundary strengthening is not distinct though the yield strength is slightly enhanced due to the formation of $(FeAl)_2B$ particles. Upon aging, precipitation of Cu-rich nanoclusters occurs, thereby resulting in enhanced strength (Fig. 4). After aging for 10 h, the B-doped steel fractured with the complete cleavage mode while the B-free steel fractured by a combination mode of cleavage and intergranular fracture, indicating that the grain boundaries were strengthened through B doping. In this aging condition, however, grain boundary fracture is not the sole reason for the poor ductility and brittle fracture. As can be seen from Fig. 3, the hardness of the steels is determined predominantly by nanocluster precipitation during aging. Thus, the high strength of the matrix induced by nanocluster precipitation leads to a brittle fracture mode for both B-doped and B-free steels. In addition, the high strength of the matrix makes it more sensitive to environmental embrittlement. As shown in Fig. 5, both steels with and without B doping showed no ductility (fractured prior to macroscopic yielding) without oil coating but ~2% and ~1% plastic elongation after oil coating respectively, a distinct improvement of ductility. These results certainly suggest that these steels are prone to environmental embrittlement. This phenomenon has been widely observed in alloys, such as FeAl [13,14], Ni_3Al [15,16], Ni_3Si [17], etc. In this case, the effect of B-doping on ductility is not substantial because environmental embrittlement and nanocluster precipitation hardening are the other factors for brittle fracture in these steels.

After aging for 200 h, the strength of both B-doped and B-free steels decreased slightly compared to the 10 h aged specimens (oil

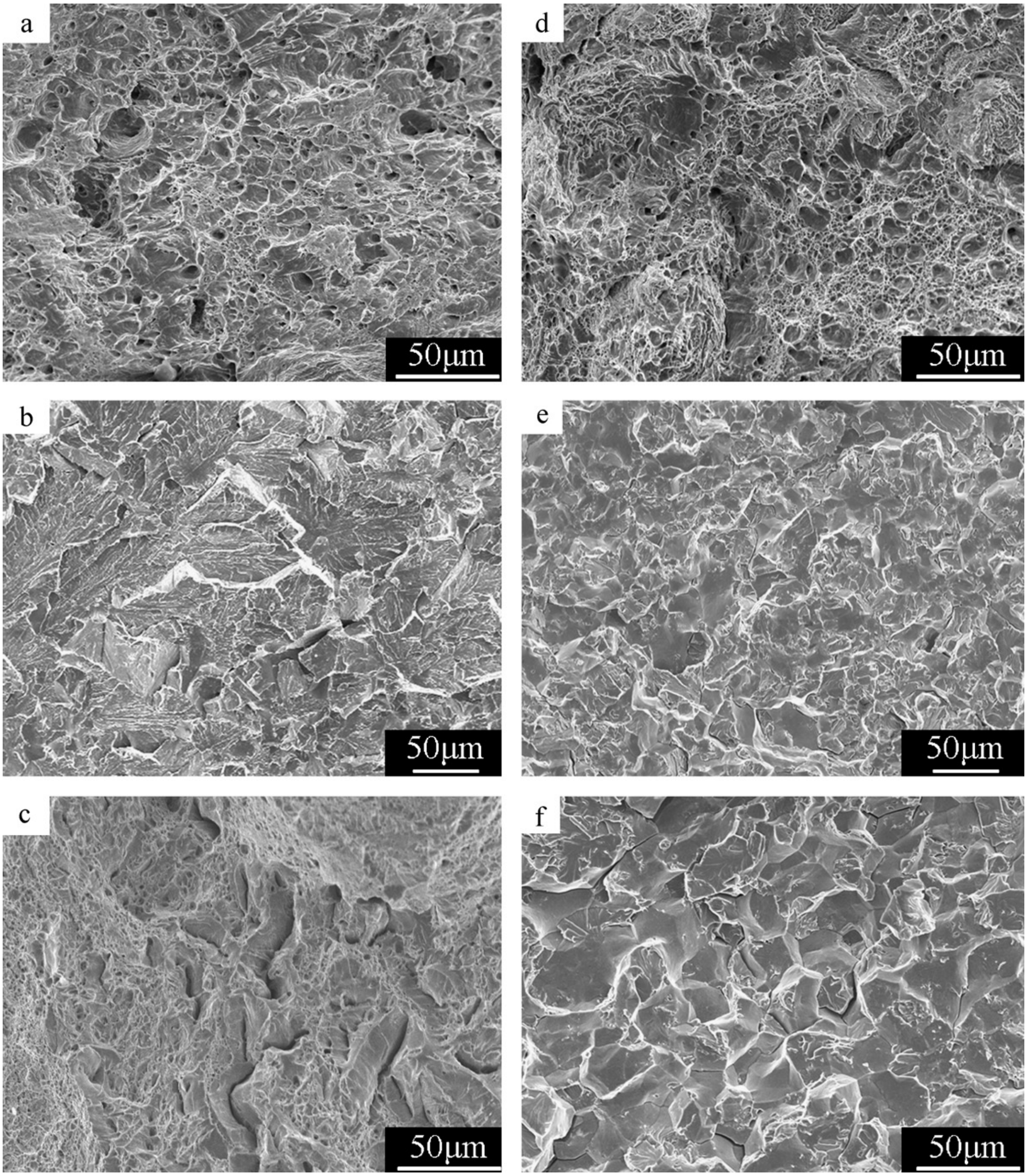

Fig. 6. Fracture surfaces of quenched B-doped and B-free samples followed by aging: (a) B-doped, as-quenched, (b) B-doped, at 500 °C for 10 h, (c) B-doped, at 500 °C for 200 h, (d) B-free as-quenched, (e) B-free, at 500 °C for 10 h and (f) B-free, at 500 °C for 200 h.

coated) due to the coarsening of Cu-rich nanoclusters [3,6,18]. The B doped steel has a higher tensile strength with ductile transgranular fracture mode while the B-free steel fails mainly by brittle intergranular fracture. This phenomenon was also observed in the room tensile tests of Co–Al–W alloys [19]. The improvement in the ductility of the nanocluster strengthened ferritic steel by B doping should be due mainly to the increase in the grain boundary cohesion arising from the boron segregation on the grain boundary.

5. Conclusions

The effects of boron and moisture-induced environmental embrittlement on the ductility of nanocluster strengthened ferritic steels were studied. Tensile tests showed that the ferritic steel with boron doping has similar yield strength but larger elongation than that without boron doping after aging for 200 h at 500 °C. There exist three mechanisms influencing the ductility of the nano-cluster-strengthened ferritic steel: (1) nano-cluster-precipitation strengthening, (2) moisture-induced embrittlement, and (3) grain boundary fracture. Boron enhances the grain boundary cohesion and suppresses intergranular fracture. Moisture-induced embrittlement can be alleviated by oil coating.

Acknowledgements

This research was supported mainly by internal funding from Auburn University and Hong Kong polytechnic University, together with the Science and Technology Development Foundation of Nanjing University of Science and Technology of China (XKF09055), the National Natural Sciences Foundation of China (No. 50871054), the Research Fund for the Doctoral Program of Higher Education of China (20093219110035), and the US National Science Foundation (CMMI-0826535).

References

[1] H.R. Habibi-Bajguirani, Mater. Sci. Eng. A338 (2002) 142.
[2] S. Vaynman, D. Isheim, R.P. Kolli, S.P. Bhat, D.N. Seidman, M.E. Fine, Metall. Mater. Trans. A39 (2008) 363.
[3] S.K. Dhua, D. Mukerjee, D.S. Sarma, Metall. Mater. Trans. 34A (2003) 241.
[4] M.E. Fine, D. Isheim, Scripta Mater. 53 (2005) 115.
[5] D. Isheim, M.S. Gagliano, M.E. Fine, D.N. Seidman, Acta Mater. 54 (2006) 841.
[6] M.K. Miller, K.F. Russell, J. Nucl. Mater. 371 (2007) 145.
[7] A.K. Sinha, Ferrous Physical Metallurgy, Butter Worth Publishers, 1989.
[8] M. Takeyama, C.T. Liu, Acta Mater. 36 (1988) 1241.
[9] C.T. Liu, E.P. George, Scripta. Metall. Mater. 24 (1990) 1285.
[10] K.N. Kim, L.M. Pan, J.P. Lin, Y.L. Wang, Z. Lin, G.L. Chen, J. Mater. Magn. Magn. Mater. 277 (2004) 331.
[11] P. Lejček, A. Fraczkiewicz, Intermetallics 11 (2003) 1053.
[12] H.G. Fu, Y.P. Lei, J.D. Xing, L.M. Huang, Ironmak. Steelmak. 35 (2008) 371.
[13] L.M. Pike, C.T. Liu, Scripta Mater. 42 (2000) 265.
[14] L.M. Pike, C.T. Liu, Intermetallics 8 (2000) 1413.
[15] C.T. Liu, Scripta Metall. Mater. 27 (1992) 25.
[16] C.T. Liu, Scripta Metall. Mater. 25 (1991) 1231.
[17] C.T. Liu, W.C. Oliver, Scripta Metall. Mater. 25 (1991) 1933.
[18] A. Machova, Mater. Sci. Eng. A319-321 (2001) 574.
[19] D. Shinagawa, T. Omori, K. Oikawa, R. Kainuma, K. Ishida, Scripta Mater. 61 (2009) 612.